Check for updates

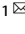## ARTICLE

Myosin 1D and the branched actin network control the condensation of p62 bodies

Xuezhao Feng[1,2,10], Wanqing Du[3,10], Mingrui Ding[4,10], Wenkang Zhao[3], Xirenayi Xirefu[1,5], Meisheng Ma[6], Yuhui Zhuang[7], Xiaoyu Fu[8], Jiangfeng Shen[7], Jinpei Zhang[1,2], Xiuying Lei[1,2], Daxiao Sun[3], Qing Xi[1,2], Yiliyasi Aisa[1,5], Qian Chen[1,2], Ying Li[3,9], Wenjuan Wang[9], Shanjin Huang[7], Li Yu[3], Pilong Li[4✉] and Na Mi[1✉]

© CEMCS, CAS 2022

Biomolecular condensation driven by liquid–liquid phase separation (LLPS) is key to assembly of membraneless organelles in numerous crucial pathways. It is largely unknown how cellular structures or components spatiotemporally regulate LLPS and condensate formation. Here we reveal that cytoskeletal dynamics can control the condensation of p62 bodies comprising the autophagic adaptor p62/SQSTM1 and poly-ubiquitinated cargos. Branched actin networks are associated with p62 bodies and are required for their condensation. Myosin 1D, a branched actin-associated motor protein, drives coalescence of small nanoscale p62 bodies into large micron-scale condensates along the branched actin network. Impairment of actin cytoskeletal networks compromises the condensation of p62 bodies and retards substrate degradation by autophagy in both cellular models and Myosin 1D knockout mice. Coupling of LLPS scaffold to cytoskeleton systems may represent a general mechanism by which cells exert spatiotemporal control over phase condensation processes.

INTRODUCTION

Biomolecular condensates, in which certain macromolecules are concentrated and others are depleted, represent an important modality and principle of membraneless organelle organization. The spatiotemporal distribution of condensates is undoubtedly critical to their functions. The formation of biomolecular condensates is often driven by liquid–liquid phase separation (LLPS) initiated by multivalent interactions between macromolecules referred to as scaffolds.[1] LLPS is highly dependent on the concentrations of scaffolds.[1–3] Equilibria between different phases and stochastic distribution of condensates can be achieved during in vitro reconstituted phase separation processes. However, cellular milieus are intrinsically non-equilibrious, crowded, and viscous systems. As such, in vivo phase separation processes are intricately controlled by local concentrations of scaffolds[4–9] and the resulting condensates are far from being uniformly or stochastically distributed throughout cells. Despite the tremendous advances made in the field of biomolecular condensates in recent years, the mechanisms to facilitate the precise spatial distribution of phase-separated condensates are still enigmatic.[10]

Dynamic and yet rigid cytoskeletal elements such as microfilaments and microtubules occupy a large amount of space within the cell. Biomolecules residing close to cytoskeletal elements[11,12] exhibit biased spatial distribution. Furthermore, active transportation by motor proteins along cytoskeletal tracks is another means to achieve inhomogeneous distributions of cargo molecules. Recent studies suggest that biomolecular condensates can promote the formation of cytoskeletal structures. The increased concentration of cytoskeletal monomers and control of the stoichiometry of regulators can influence local nucleation rates and filament growth.[4,9,13–16] However, it remains unclear whether cytoskeletal dynamics can directly regulate cytosolic condensates within a cell.[17,18]

We and others previously showed that the branched actin network plays important roles in autophagy, including shaping the isolation membrane.[19,20] Phase separation also plays critical roles in autophagy.[21–23] p62/SQSTM1, a well-known selective autophagy receptor, mediates phase separation of poly-ubiquitinated proteins into larger condensates, also known as p62 bodies. p62 and poly-ubiquitinated proteins are the scaffolds for the formation of p62 bodies. Subsequently, p62 bodies are sequestered in autophagosomes and also act as nucleation sites for autophagy.[23,24] Here we sought to reveal the regulatory effect of cytoskeletal elements on autophagy in general and on the condensation of p62 bodies in particular.

---

[1]State Key Laboratory of Pathogenesis, Prevention and Treatment of Central Asian High Incidence Diseases, Clinical Medical Research Institute, The First Affiliated Hospital of Xinjiang Medical University, Urumqi, Xinjiang, China. [2]Basic Medical College, Xinjiang Medical University, Urumqi, Xinjiang, China. [3]State Key Laboratory of Membrane Biology, Tsinghua University-Peking University Joint Center for Life Sciences, School of Life Sciences, Tsinghua University, Beijing, China. [4]Beijing Advanced Innovation Center for Structural Biology & Frontier Research Center for Biological Structure, Tsinghua University-Peking University Joint Center for Life Sciences, School of Life Sciences, Tsinghua University, Beijing, China. [5]College of Pharmacy, Xinjiang Medical University, Urumqi, Xinjiang, China. [6]Tongji Medical College of Huazhong University of Science and Technology, Wuhan, Hubei, China. [7]Center for Plant Biology, School of Life Sciences, Tsinghua University, Beijing, China. [8]Ministry of Education Key Laboratory of Protein Sciences, Beijing Advanced Innovation Center for Structural Biology, Beijing Frontier Research Center of Biological Structures, School of Life Sciences, Tsinghua University, Beijing, China. [9]Center of Biomedical Analysis, Tsinghua University, Beijing, China. [10]These authors contributed equally: Xuezhao Feng, Wanqing Du, Mingrui Ding. ✉email: pilongli@mail.tsinghua.edu.cn; mina2a@163.com

RESULTS

The Arp2/3-derived branched actin network is required for the formation of p62 bodies

We treated wild-type (WT) normal rat kidney (NRK) cells with the antibiotic puromycin, a reagent commonly used to generate ubiquitin-positive aggregates and p62 bodies in cells,[25] and indeed we found an increased number of p62 bodies upon puromycin treatment (Supplementary information, Fig. S1a, b). To determine whether cytoskeleton structures and components are involved in regulating the formation of p62 bodies, we first applied a number of pharmacological reagents to perturb various cytoskeletons in cells, including cytochalasin B (actin polymerization inhibitor), blebbistatin (an inhibitor of nonmuscle myosin II), CK666 (an inhibitor of Arp2/3 complex and actin polymerization)[26] and nocodazole (a highly specific anti-microtubule reagent). We found that cytochalasin B and CK666 can strongly prevent the formation of p62 bodies in puromycin-treated NRK cells, whereas blebbistatin and nocodazole have weak or no effect (Fig. 1a, b; Supplementary information, Fig. S1c, d). This suggests the importance of the actin network, especially the Arp2/3-derived branched actin network, in p62 body formation. Similar results were observed in 8 other cell lines (Supplementary information, Fig. S1e, f), indicating that the effects of the branched actin network perturbation on the formation of p62 bodies are general. Although p62 body formation was significantly inhibited, the levels of ubiquitinated proteins and p62 itself were not affected upon CK666 addition in the presence of puromycin (Fig. 1c), indicating a defect of the p62 body assembly process but not of the condensate scaffolds per se. p62 bodies dissolved rapidly upon addition of 1,6-hexanediol, a chemical known to disrupt many LLPS assemblies, and reappeared after the chemical was washed away. However, p62 bodies did not reappear in cells treated with CK666 even after the removal of 1,6-hexanediol, suggesting a pivotal role of the branched actin network in the condensation of p62 bodies. The suppression effect was restored only after both CK666 and 1,6-hexanediol were washed off (Supplementary information, Fig. S1g, h). These results together indicate that the branched actin network may play important roles in the formation of p62 bodies.

We next used confocal fluorescence microscopy to examine the spatial relationship between the branched actin network and p62 bodies. In puromycin-treated cells, p62 bodies were highly colocalized with actin structures (Fig. 1d). To further validate this observation, we transfected cells with GFP-p62 and LifeAct-mRFPruby, a widely used probe for polymerized actin fibers.[27] Live-cell imaging showed that LifeAct puncta were colocalized with p62 bodies (Fig. 1e). Individual p62 bodies appeared throughout the branched actin network (Supplementary information, Fig. S1i). We further confirmed the proximity of actin and p62 bodies using an APEX2-IP technique[28] (Fig. 1f). To evaluate the ultrastructure of the p62 condensates, we scrutinized them by transmission electron microscopy (TEM) using APEX2-GFP-p62. This approach also revealed that p62 bodies were closely associated with filamentous structures (Fig. 1g). Overall, these pieces of evidence indicate that p62 bodies likely assemble along branched actin networks.

The Arp2/3 complex is essential for the formation of p62 bodies

The formation of branched actin networks requires activation of the branched actin nucleator Arp2/3 complex, which binds to actin filaments and forms the first subunit of a new branch.[29] To better understand the role of branched actin in p62 phase separation, we analyzed the roles of two subunits, Arpc2 and Arpc1b, of the branched actin nucleator Arp2/3 complex. Colocalization was further confirmed by co-expressing Arpc2-GFP and tdTomato-p62 in NRK cells (Fig. 2a). After puromycin treatment, p62 bodies were colocalized with Arpc2 in NRK cells

(Fig. 2b) and A549 cells (Supplementary information, Fig. S2a). Time-lapse live-cell imaging showed that actin and Arpc1b were also colocalized with p62 bodies in NRK cells (Supplementary information, Fig. S2b and Video S1). We further knocked down Arpc2 in NRK cells using short hairpin RNA (shRNA) and found that the formation of p62 bodies was severely compromised (Fig. 2c–e; Supplementary information, Fig. S2c–e). In addition, the absence of p62 bodies was not due to decreased concentrations of their two major scaffolds as the level of ubiquitinated proteins was much higher in Arpc2 knockdown (KD) cells regardless of puromycin treatment while the level of p62 was largely unaltered (Fig. 2f; Supplementary information, Fig. S2f). Accordingly, ectopic expression of Arpc2-Myc (Fig. 2c–e) rescued the defect in the formation of p62 bodies due to shArpc2 treatment (Fig. 2c–e). Collectively, these data indicate that Arp2/3 complex and branched actin networks are required for the formation of p62 bodies.

Myosin 1D coalesces with p62 bodies

We next tried to examine whether actin-associated motor proteins play a role in p62 phase separation.[30] Among six type I myosin homologs tested, we found that Myo1D,[31] and to a lesser degree Myo1B, was colocalized with p62 bodies in NRK cells (Fig. 3a; Supplementary information, Fig. S3a–c) and A549 cells (Supplementary information, Fig. S3d). We then focused on Myo1D in the following analysis. The large Myo1D condensates were dispersed upon treatment with 1,6-hexanediol and re-condensed with p62 upon removal of 1,6-hexanediol (Supplementary information, Fig. S3e, f). The endogenous colocalization between Myo1D and p62 bodies was further revealed in Atg12 knockout (KO) NRK cells, in which autophagosomes cannot degrade p62 bodies (Supplementary information, Fig. S3g). To visualize the location of Myo1D more precisely, we used structured illumination microscopy (SIM) to obtain super-resolution images. SIM images of Myo1D and p62 also confirmed that Myo1D was colocalized with p62 bodies (Fig. 3b, c). Time-lapse live-cell imaging revealed that Myo1D-containing p62 bodies fused upon contact and relaxed to spherical shapes, suggesting the fluidity of p62 bodies (Fig. 3d; Supplementary information, Video S2), consistent with previous reports.[21] Using a peroxidase-mediated proximity labeling technique coupled with TEM,[28] we also confirmed the presence of APEX2-GFP-Myo1D inside membraneless electron-dense foci (Fig. 3e). Furthermore, correlative light electron microscopy (CLEM) analysis revealed that Myo1D and p62 were colocalized in condensates, which are presumably p62 bodies (Supplementary information, Fig. S3h).

Next, we performed fluorescence recovery after photobleaching (FRAP) experiments to visualize the fluidity of Myo1D and p62 within the condensates in cells. We found that both proteins could recover after photobleaching and Myo1D recovered much faster than p62 (Fig. 3f, g). The different recovery rates imply that p62 is a scaffold and myosin 1D is a client in the condensates. In test tubes, poly-ubiquitin (poly-Ub, ub8) along with p62, but not p62-ΔPB1 (with deletion of the self-oligomerization domain), can undergo LLPS to assemble p62 bodies in vitro.[21] Interestingly, Myo1D can be incorporated into these reconstituted p62 bodies (Supplementary information, Fig. S4a). Consistent with our observation in cells (Fig. 3a), these Myo1D-containing p62 condensates were able to fuse with each other and relax towards spherical shapes, indicating their liquidity in vitro (Fig. 3h).

Myo1D contains a head (motor) domain, a neck domain, and a tail domain. The neck region contains IQ domains, which provide binding sites for Calmodulin. The tail domain is composed of a myosin-I family tail homology 1 (TH1) domain.[32,33] To dissect the molecular details of interactions between Myo1D and p62 condensates, we accessed a series of truncations of Myo1D (Fig. 3i). Using purified recombinant proteins, we showed that the IQ and TH1 structural domains, either alone or together, were co-
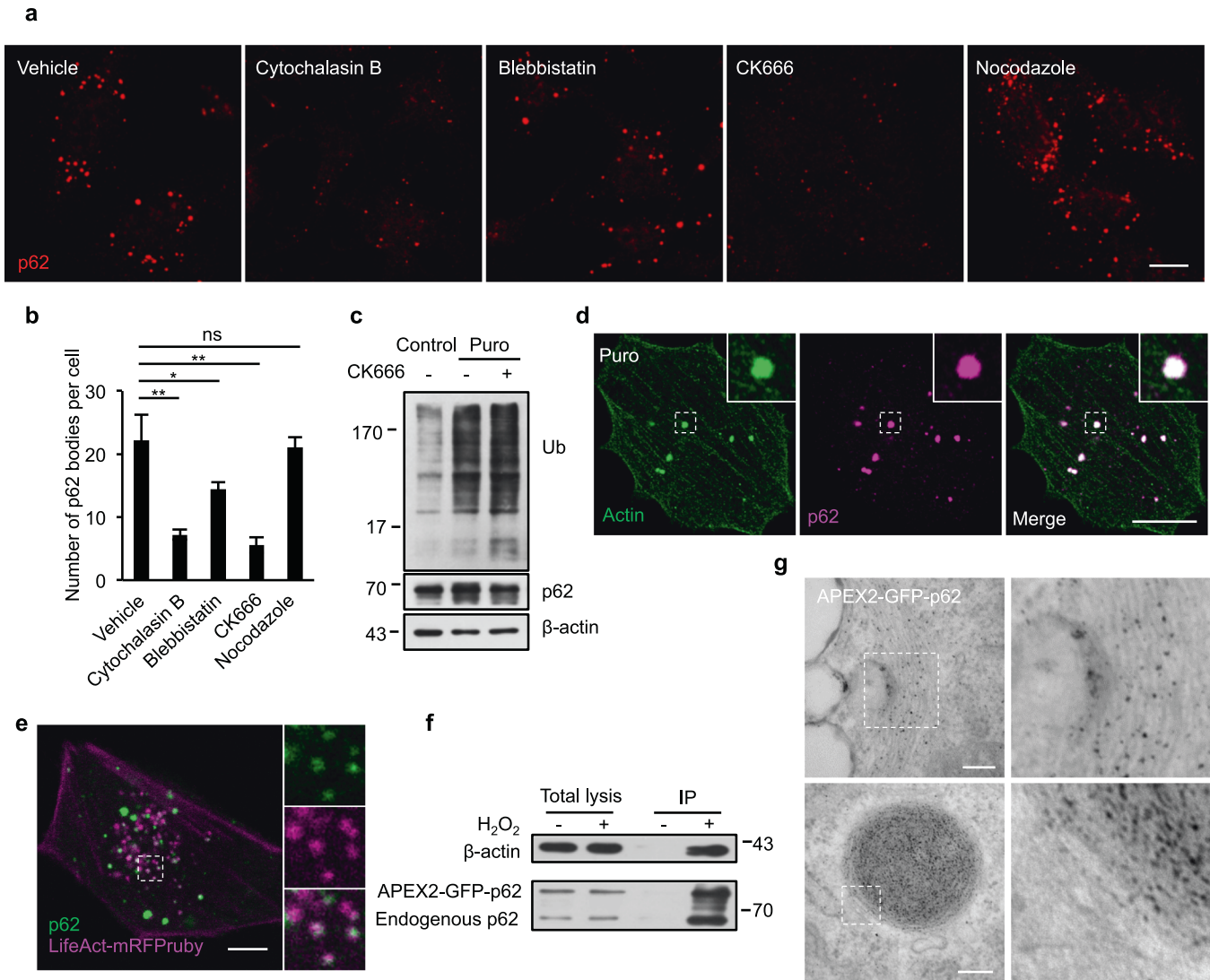
Fig. 1 The Arp2/3-derived branched actin network is required for the formation of p62 bodies. a NRK cells treated with puromycin were incubated with vehicle (DMSO), cytochalasin B (1 µM), blebbistatin (20 µM), CK666 (100 µM) or nocodazole (25 µM), and stained with an antibody against p62. Scale bar, 5 µm. **b** The number of p62 bodies was quantified in cells from **a** (3 independent experiments; 50 cells were assessed per independent experiment). P-values were calculated using the two-tailed unpaired t-test. $*P < 0.05$; $**P < 0.01$. **c** Cells were untreated (control) or treated with 1 mg/mL puromycin with or without CK666 for 8 h, and the cell lysates were analyzed by western blotting with antibodies against ubiquitin and p62. **d** Cells were transfected with GFP-actin and treated with puromycin for 8 h, then stained with anti-GFP and anti-p62 antibodies. Scale bar, 10 µm. **e** NRK cells were transfected with GFP-p62 and LifeAct-mRFPruby and fluorescence signals were visualized. Scale bar, 10 µm. **f** APEX2-GFP-IP was performed using NRK cells stably expressing APEX2-GFP-p62. The immunoprecipitate was analyzed by western blotting with antibodies against actin and p62. **g** TEM images showing the diaminobenzidine (DAB) staining pattern of NRK cells transfected with APEX2-GFP-p62. Scale bar, 200 nm. The boxed region, containing filamentous structures, is magnified to the right.

sedimented with poly-Ub/p62 complexes, albeit to a lesser degree than full-length (FL) Myo1D (Fig. 3j). Consistent with this, Myo1D and its domain truncations were also incorporated into reconstituted p62 bodies in test tubes, whereas Myo1D alone did not accumulate in the pellet after centrifugation (Supplementary information, Fig. S4b, c). When expressed in cells, these truncated Myo1D proteins were colocalized with p62 bodies (Supplementary information, Fig. S4d). Taken together, our data show that Myo1D can coalesce with liquid-like p62 condensates both in vitro and in vivo, likely via physical interaction of the IQ and TH1 domains with poly-Ub/p62 complexes.

Myo1D promotes the coalescence of p62 bodies
To test whether Myo1D is necessary for the formation of p62 bodies in vivo, we generated a Myo1D KO NRK cell line. Large micron-scale

p62 bodies failed to form in Myo1D KO cells, even though the levels of p62 and ubiquitinated proteins were not decreased (Fig. 4a–d; Supplementary information, Fig. S5a). Instead, p62 mainly formed nanometer-scale condensates, at least 10-fold smaller than large p62 bodies, in Myo1D KO cells as shown by proximity labeling coupled with TEM (Fig. 4e). Similar phenomena were also observed in multiple Myo1D KO cell clones based on immunofluorescence staining (Supplementary information, Fig. S5b–d). We then ectopically expressed the p62 S403E mutant in cells, which mimics S403 phosphorylation and can promote the formation of p62 bodies.[21] p62 S403E mutant also failed to form large condensates in Myo1D KO cells (Supplementary information, Fig. S5e–g).

To assess the mechanism by which Myo1D participates in the formation of p62 bodies, we expressed GFP-fused WT Myo1D and variants, including the K108R mutant and the above-mentioned
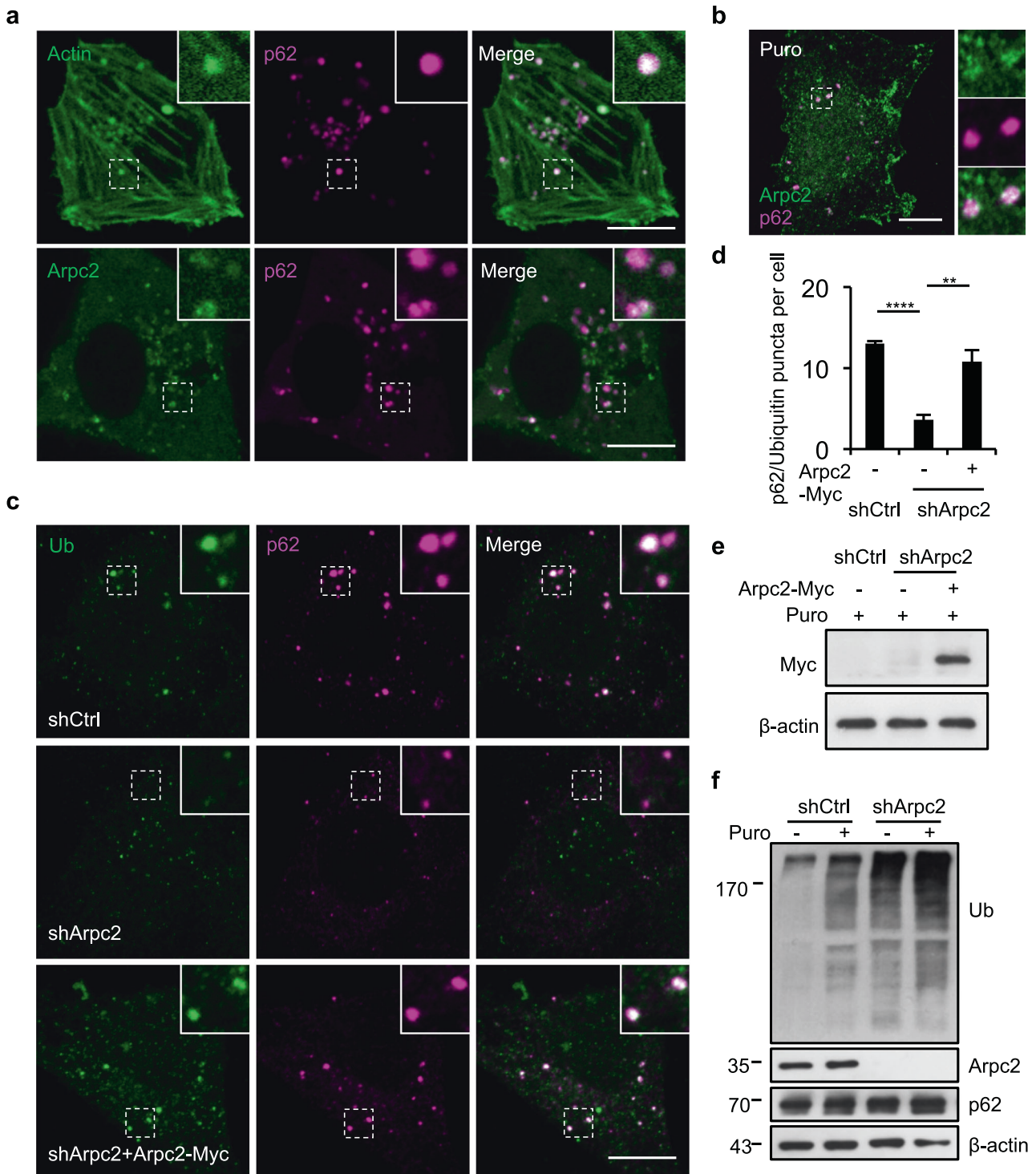
Fig. 2 The Arp2/3 complex is essential for the formation of p62 bodies. a Cells were transfected with GFP-Actin or Arpc2-GFP together with tdTomato-p62, and then imaged. Regions containing p62 foci that co-localize with branched actin filaments are outlined with white dashed lines and are magnified in the insets. Scale bars, 10 μm. **b** Cells were treated with 1 mg/mL puromycin for 8 h and stained with antibodies against Arpc2 and p62. Scale bar, 10 μm. **c** NRK cells expressing non-targeting control shRNA (shCtrl), Arpc2 shRNA, or Arpc2 shRNA plus shRNA-resistant Arpc2-Myc cDNA were treated with 1 mg/mL puromycin for 8 h, and then stained with ubiquitin and anti-p62 antibodies. Scale bar, 10 μm. **d** The number of puncta positive for both ubiquitin and p62 was quantified in cells from **c** ($n = 3$ independent experiments; 50 cells were assessed per independent experiment). *P*-values were calculated using the two-tailed unpaired *t*-test. ***P < 0.01; ****P < 0.0001. **e** Immunoblot showing the protein expression level in NRK cells with ectopic expression of Myc-tagged Arpc2. **f** NRK cells expressing shCtrl or Arpc2 shRNA were treated with 1 mg/mL puromycin for 8 h, and the cell lysates were analyzed by western blotting with antibodies against ubiquitin, Arpc2, β-actin, and p62.
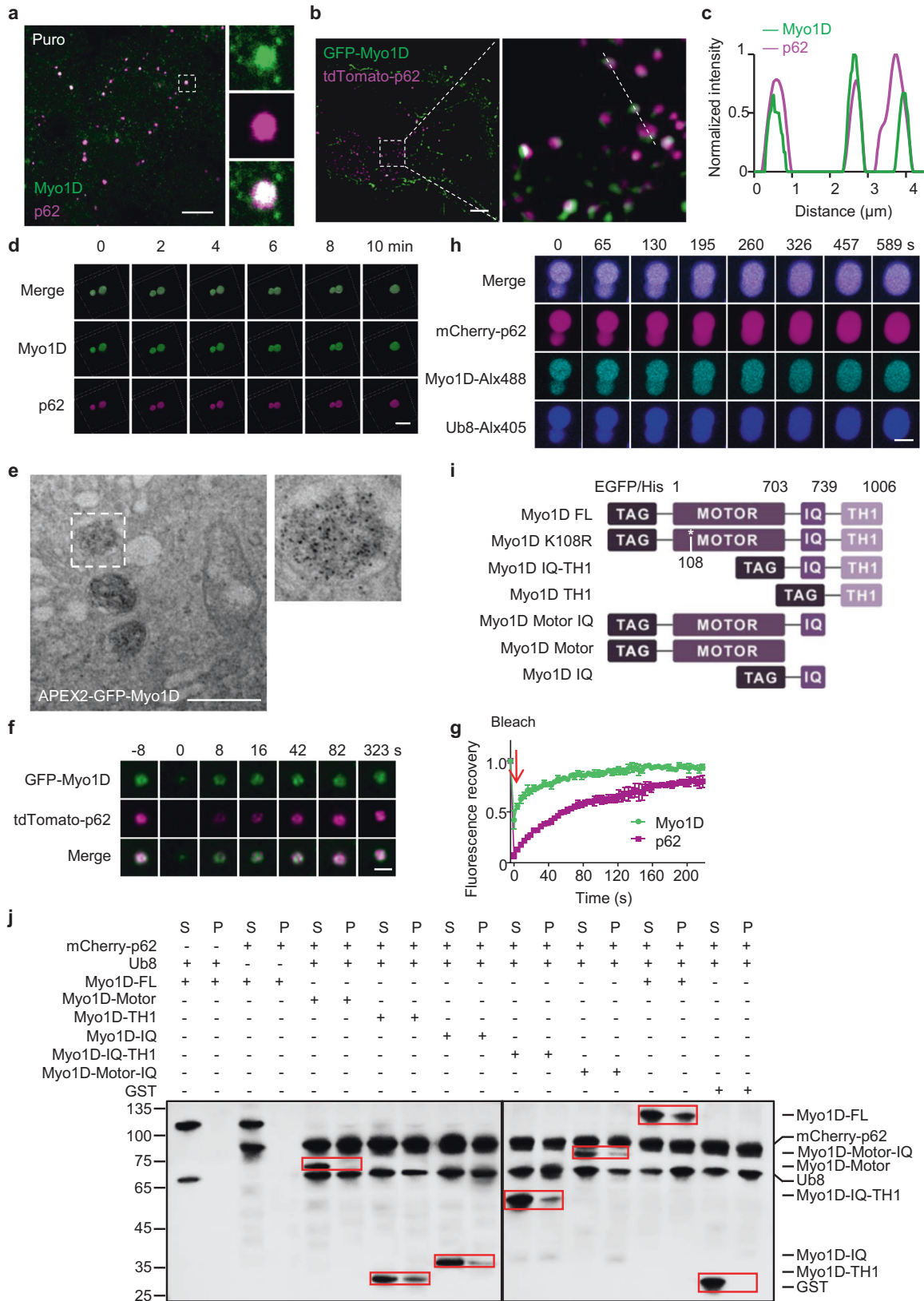
truncations, in Myo1D KO cells (Fig. 3i). K108R is the 'rigor' mutant of Myo1D, in which the motor function is abolished by a single point mutation in the ATP-binding site. The reduction of p62 bodies in Myo1D KO cells was rescued by ectopic expression of FL

Myo1D (Fig. 4f). Although the IQ domain, the TH1 domain, the Motor-IQ domain and the IQ-TH1 domain were able to partition into small p62 bodies, they failed to induce coalescence of these small condensates into large p62 bodies (Fig. 4f; Supplementary

Fig. 3 Myosin 1D coalesces with p62 bodies. a NRK cells were treated with 1 mg/mL puromycin for 8 h, and stained with antibodies against Myo1D and p62. Scale bar, 10 μm. **b** NRK cells were transfected with GFP-Myo1D and tdTomato-p62, and observed by SIM. Scale bar, 10 μm. **c** Line profiling of a representative section of the cell, indicated by the white dashed line in **b**. **d** Time-lapse images of p62 bodies in live ATG12 KO NRK cells transiently expressing GFP-Myo1D and tdTomato-p62. Scale bar, 1 μm. **e** TEM image showing the DAB staining pattern in NRK cells transiently transfected with APEX2-GFP-Myo1D and tdTomato-p62. Scale bar, 1 μm. **f** Fluorescence intensity recovery of a p62 body in an NRK cell transiently expressing GFP-Myo1D and tdTomato-p62 after photobleaching. Scale bar, 1 μm. **g** Quantification of fluorescence intensity recovery of a photobleached p62 body ($n = 3$). **h** Droplets formed by LLPS of p62 (10 μM), Ub8 (6 μM) and Myo1D (1 μM) fusion upon contact in vitro. Scale bar, 5 μm. **i** Schematic diagram of Myo1D constructs. EGFP was fused to the N-terminus of FL Myo1D, Myo1D K108R, Myo1D IQ-TH1, Myo1D TH1, Myo1D Motor-IQ or Myo1D IQ. **j** Representative sedimentation analysis showing Myo1D fragments concentrated in the soluble phase (S) or condensed phase (P). Results were analyzed by western blotting using anti-His tag antibody.

information, Fig. S6a). This indicates that the integrity of Myo1D is essential to drive coalescence of small nanoscale p62 bodies into large micron-scale p62 condensates. Importantly, the motor-defective mutant GFP-Myo1D K108R failed to rescue the KO effect, indicating that the motor activity of Myo1D is required for the proper formation of p62 bodies in vivo (Fig. 4f).

We further set up an in vitro reconstitution assay to determine whether and how Myo1D directly promotes p62 condensation. We established an Arp2/3-derived branched actin network and generated p62 bodies using p62 and poly-Ub[9,21] (Fig. 4g). To initiate actin polymerization, we added 1 μM actin (50% Oregon-green labeled), 100 nM Arp2/3 complex, 600 nM capping protein (CapZ), and 300 nM PWCA (a domain consisting of a conserved C-terminal proline-rich region and WASP homology 2 peptides plus a connector and acidic segments, which promotes Arp2/3-mediated actin polymerization[34]). This led to robust actin polymerization in the plane of the chambered cover glass, as observed by total internal reflection fluorescence (TIRF) microscopy. Myo1D was subsequently added to the solution (Fig. 4g). We observed the formation of p62 bodies on the Arp2/3-derived microfilaments (Fig. 4h, i; Supplementary information, Fig. S6b, c). In addition, the reconstituted p62 bodies were observed by scanning electronic microscopy (SEM) (Fig. 4j; Supplementary information, Fig. S6d). Consistent with the finding that Myo1D can colocalize with branched actin network in cells (Supplementary information, Fig. S6e), Myo1D also colocalized with reconstituted branched actin network in the presence or absence of p62, indicating that Myo1D may bring p62 to the branching sites of actin to elevate its local concentration for further condensation (Supplementary information, Fig. S6f). During in vitro reconstitution assays, p62 condensate formation dramatically decreased with significantly smaller size for K108R Myo1D mutant compared to WT Myo1D (Supplementary information, Fig. S6g). Furthermore, ATP is required for p62 condensation during in vitro assays (Supplementary information, Fig. S6h). These data suggest that Myo1D's motor activity may also play a role in further tethering p62/Ub along branched actin network and promoting condensate formation among nanoscale environment, despite that Myo1D is a non-processive motor and may not carry out long-range transportation. Although Myo1D alone cannot accelerate p62 body phase separation, the addition of Myo1D contributes significantly to this process in the presence of the Arp2/3-derived branched actin network (Fig. 4k; Supplementary information, Fig. S6i). These data indicate that Myo1D drives coalescence of small nanoscale p62 bodies into large micron-scale condensates along the branched actin network.

The branched actin network regulates autophagy by harnessing p62 phase condensation

p62 mediates the phase separation of ubiquitinated proteins into larger condensates for autophagic degradation.[35] Our previous study showed that branched actin networks are required for autophagy.[19] Interestingly, large p62 bodies colocalized with LC3 whereas tiny discrete nanoscale p62 bodies barely colocalized with LC3 (Fig. 5a–c). These results support the idea that there is likely a minimal size of p62 condensates for further progression of autophagy.[23] Next, we investigated whether or not the branched actin network facilitates autophagy by regulating p62

condensation. Using Arpc2 KD cells and Myo1D KO cells, we found that the decrease of Arpc2 or the absence of Myo1D markedly attenuated autophagy as determined by the impaired degradation of p62 (Fig. 5d, e; Supplementary information, Fig. S7a, b).

In cells lacking Myo1D or with reduced Arpc2, p62 was dispersed in numerous smaller p62 puncta and was less colocalized with LC3, compared with control cells (Fig. 5f, g). TEM analysis confirmed that in Myo1D KO cells, the formation of large p62 bodies was blocked, and p62 formed small nanoscale condensates (Fig. 5h). These discrete puncta surrounded the edge of the autophagosomes but could not be packaged into the mature autophagosome structures (Fig. 5h). Ectopic expression of Myc-Myo1D rescued the defect in the formation of large p62 bodies during autophagy due to Myo1D KO (Supplementary information, Fig. S7c, e). On the other hand, ubiquitin-modified proteins in WT cells are significantly reduced when puromycin is eluted, but there is still a large accumulation in Myo1D KO cells, indicating that Myo1D is required for appropriate degradation of ubiquitinated proteins (Fig. 5i; Supplementary information, Fig. S7f). Furthermore, we generated Myo1D KO mice. Accumulation of ubiquitinated protein was detected in these mice (Fig. 5j). These results indicate that malfunction of the branched actin network or its motor protein Myo1D can cause stalling of p62 condensation, which subsequently leads to defective autophagy.

Together, the data above allow us to make the following proposals. Firstly, the local concentrations of p62 body scaffolds (i.e., p62 and poly-ubiquitinated protein) in normal cells are below the critical concentrations for phase separation. Secondly, upon certain stimuli which lead to p62 condensation (e.g., starvation), the affinity between motor and cytoskeleton and an ATP-dependent cargo gathering mechanism mediated by motor proteins allows elevation of the scaffold concentrations along branched actin networks, thereby promoting the coalescence of small nanoscale p62 condensates into large micron-scale p62 bodies. Thirdly, only large p62 bodies can be packaged into mature autophagosome and subjected to degradation (Fig. 5k). The formation of large micron-scale p62 bodies is severely impaired in cells lacking motors or branched actin networks.

DISCUSSION

LLPS is an appealing mechanism for the biomolecular condensation and formation of membraneless organelles that exerts important physiopathological functions in cells.[1,2,4,23,36] Cells must spatiotemporally arrange their contents to ensure that LLPS and condensation occur in the right place at the right time. Rigid cytoskeleton networks play fundamental roles in arranging cellular contents within limited space. Here, we demonstrate that Arp2/3-derived branched actin networks are associated with p62 bodies and required for the formation of functional p62 bodies, a key ubiquitinated protein-containing condensate en route to lysosome degradation in autophagy. Asymmetrically distributed actin structures provide a spatial positioning system with locally increased concentrations of molecules to facilitate assembly of p62 condensates. Moreover, the motor protein Myo1D can
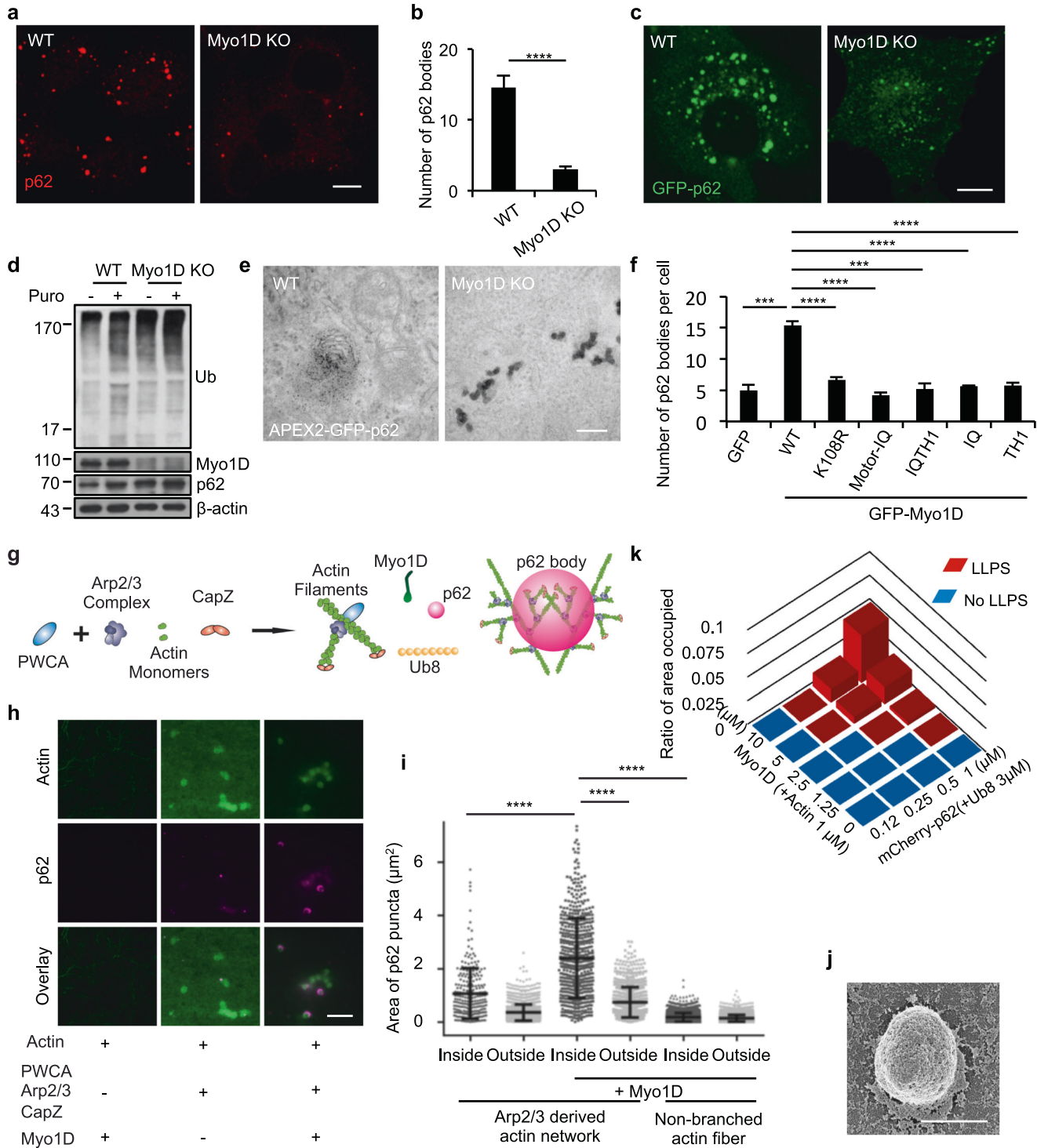
actively recruit small nanoscale p62 bodies towards the branched actin networks. Such ATP-dependent cargo gathering mechanism along spatially positioned actin tracks elevated local concentrations of p62 scaffold for LLPS and increased proximity between small p62 condensates for further coalescence into large p62 bodies (Fig. 5k). The functional distinction between large and small p62 bodies highlighted that size distribution of condensates can be controlled by cytoskeleton dynamics and is critical for certain essential cellular processes such as autophagy. Coupling of scaffolds to prominent cellular systems (such as cytoskeleton and motor protein systems (this study), membrane and membrane-

tethering proteins,[37,38] and chromatin loci and chromatin-associated protein and RNAs[39]) elevates the local scaffold concentrations for LLPS and condensation. This is likely a general mechanism by which cells exert spatiotemporal control over phase condensation and coalescence processes.

MATERIALS AND METHODS
Cell culture, transfection, and plasmids
NRK cells were obtained from the American Type Culture Collection (ATCC). Cells were cultured in Dulbecco's Modified Eagle Medium (DMEM; Life

Fig. 4 Myo1D promotes the formation of p62 bodies. a Representative images of WT NRK cells and Myo1D KO cells treated with 1 mg/mL puromycin for 8 h and stained with an antibody against p62. Scale bar, 10 μm. **b** The number of p62 bodies was quantified in cells from **a** ($n = 3$ independent experiments; over 50 cells were assessed per independent experiment). The P-value was calculated using the two-tailed unpaired t-test. ****$P < 0.0001$. **c** WT and Myo1D KO NRK cells were transfected with GFP-p62. Scale bar, 10 μm. **d** WT and Myo1D KO NRK cells were treated with 1 mg/mL puromycin for 8 h, and the cell lysates were analyzed by western blotting with antibodies against ubiquitin and p62. **e** TEM images showing the DAB staining pattern in WT or Myo1D KO NRK cells transiently transfected with APEX2-GFP-p62. Scale bar, 200 nm. **f** The number of p62 bodies was quantified in WT or Myo1D KO cells transfected with the indicated Myo1D truncations and mutants. Cells were treated with puromycin and then stained with antibodies against GFP and p62 (3 independent experiments; 50 cells were assessed per independent experiment). P-values were calculated using the two-tailed unpaired t-test. *$P < 0.05$; **$P < 0.01$. **g** Schematic drawing of the p62 body reconstitution assay. Molecules are not drawn to scale. **h** TIRF images showing that p62 body formation (middle) depends on actin polymerization and Myo1D. PWCA (300 nM), actin (1 μM, 50% Oregon-green labeled), Arp2/3 complex (100 nM), and CapZ (600 nM) were pre-loaded into the chamber. Then Myo1D (100 nM), p62 (0.5 μM), and Ub8 (3 μM) were added into the reconstitution system. Scale bar, 5 μm. **i** Quantification of the area of p62 puncta (μm^2) inside and outside of actin phase-separated clusters from images in **h** (3 independent experiments; over 100 puncta were assessed per independent experiment). P-values were calculated using the two-tailed unpaired t-test. ****$P < 0.0001$. **j** SEM image showing the structure of a reconstituted p62 body on the Arp2/3-derived actin network. Scale bar, 1 μm. **k** A phase diagram of p62, Ub8 and Myo1D in the indicated concentration ranges.

Technologies, 11960) supplemented with 10% fetal bovine serum (FBS; BI, 04-002-1A-US) and 50 μg/mL penicillin/streptomycin, and maintained at 37 °C under 5% CO_2. For starvation, cells were washed twice with phosphate-buffered saline (PBS) and incubated in starvation DMEM medium (Life Technologies, 11960) or Dulbecco's Phosphate-Buffered Saline (DPBS; Gibco, 14287) for the indicated time. NRK cells were transfected with 3 μg DNA via Amaxa nucleofection using solution T and program X-001. The GFP-FL Myo1D constructs were generated by cloning Rattus norvegicus Myo1D (NCBI accession number: 25485) into pEGFP-C1 vector. The plasmids FL Myo1D (amino acid (aa) 1–1006), Myo1D K108R (aa 1–1006) and Myo1D Motor-IQ (aa 1–739) were constructed using pEGFP-C1 vector as the backbone. Arpc2-GFP was constructed using pEX-1 vector as the backbone. The EGFP sequence was then replaced with Myc tag. For rescue experiments, an shRNA-resistant allele of ARPC2 was generated via mutation. The mCherry-Myo1D construct was generated by cloning rat Myo1D cDNA into pmCherry-C1 vector. The shRNA sequences targeting rat Arpc2 are 5′-GCTGGCATGTTGAAGCGAAATTGTT-3′ and 5′-CGGGACTATCTGCACTACCA-CATTA-3′ (Vector backbone pGPU6/Neo). The CRISPR/Cas9 vector backbone is PX458 (48138, Addgene). The gRNA sequences targeting rat Myosin 1D are 5′-GTGCTGAACATCTATGGAA-3′ and 5′-TTTCCGTGAACCCATACA-3′. The His6-Myo1D Motor-IQ was generated by cloning Rat Myo1D motor IQ (aa 1–739) into pET21b. GFP-actin, Arpc1b-Cherry and GFP-p62 constructs were generated previously. The LifeAct-mRFPruby was provided by W. Liu's laboratory. tdTomato-p62 plasmid was a gift from Dr. Terje Johansen. EGFP-Myo1A, EGFP-tagged Myo1D IQ-TH1 (aa 570–1006), Myo1D IQ (aa 694–747), or Myo1D TH1 (aa 748–1006) were gifts from Dr. Matthew J. Tyska.[32] EGFP-Myo1D IQ (aa 694–747), His6-Myo1D IQ-TH1 (aa 570–1006), His6-Myo1D IQ (aa 694–747), Myo1D Motor (aa 1–703) and His6-Myo1D TH1 (aa 748–1006) constructs were provided by Dr. Qing Lu.

Inhibitors and reagents
Cells were incubated with fresh DMEM medium supplemented with 10% FBS and 50 μg/mL penicillin/streptomycin for 12–18 h. Formation of p62 bodies was induced by puromycin (1 mg/mL; Sigma Aldrich, 58-58-2). Cells were treated with puromycin and pharmacological inhibitors (CK666, 100 μM, Sigma Aldrich, 442633-00-3; blebbistatin, 20 μM, Sigma Aldrich, 1177356-70-5; cytochalasin B, 1 μM, Sigma Aldrich, 14930-96-2; or nocodazole, 25 μM, Sigma Aldrich, 31430-18-9) for 8 h. 1,6-Hexanediol (2%, Sigma Aldrich, 629-11-8) was added to NRK cells for 20 min.

Immunoblotting
Cells were washed with ice-cold PBS and lysed in dishes with lysis buffer (50 mM Tris-HCl, pH 7.4, 2% SDS and 2 mM EDTA, pH 8.0), and then mixed with 5× SDS-PAGE loading buffer (0.6 M Tris-HCl, pH 6.8, 2% SDS, 25% glycerol, 14.4 mM DTT and 0.1% bromophenol blue) and boiled at 100 °C for 15 min. Cell lysates were separated on 10% SDS-PAGE gels. Proteins were transferred to nitrocellulose membrane (PALL NT nitrocellulose, 66485) and blocked with 5% skim milk (BD, 232100) in PBS for 2 h at room temperature, followed by antibody incubation in Solution 1 (TOYOBO Immunoreaction Enhancer Solution, NKB-201). Rabbit anti-actin (Sigma Aldrich, A2066; 1:50,000), rabbit anti-p62 (MBL, PM045; 1:1000), mouse anti-Myosin 1D (Santa Cruz, SC-515292; 1:100), mouse anti-Arpc2 (Santa Cruz, SC-515754; 1:1000), and mouse anti-ubiquitin (Cell Signaling Technology, 3936S; 1:5000) were used as primary antibodies. Incubation was carried out for 1 h at room temperature. After 4 washes with PBST

buffer, membranes were incubated with goat anti-rabbit (Southern Biotech, 4010-05; 1:5000) or goat anti-mouse (Southern Biotech, 1070-05; 1:5000) secondary antibody for 1 h at room temperature. After extensive washing with PBST, membranes were finally exposed to the X-ray film.

Immunostaining and confocal fluorescence microscopy
WT, Myo1D KO, or Arp2 KD NRK cells were grown on coverslips. After treatment, cells were washed with PBS, fixed in 4% paraformaldehyde for 10 min, and then washed with PBS three times for 10 min each. Cells were permeabilized by incubating in PBS containing 0.1% saponin for 10 min. After blocking with goat serum in PBS for 30 min, cells were stained with primary antibody in blocking buffer for 1 h, and washed with PBS three times. The primary antibodies used were as follows: mouse anti-GFP (Roche, 11814460001; 1:500), rabbit anti-p62 (MBL, PM045; 1:1000), rabbit anti-LC3 (MBL, PM036, PM046; 1:500), mouse anti-Myosin 1D (Santa Cruz, SC-515292; 1:50), rabbit anti-Myosin 1D (Santa Cruz, SC-515292; 1:50), rabbit anti-Myosin 1D (LSBio, LS-C356202; 1:500), mouse anti-Myosin 1B (Santa Cruz, SC-393053; 1:50), mouse anti-Myosin 1C (Santa Cruz, SC-136544; 1:50), mouse anti-Myosin 1E (Santa Cruz, SC-293354; 1:50), or mouse anti-Myosin 1F (Santa Cruz, SC-376534; 1:50), mouse anti-Arpc2 (Santa Cruz, SC-515754; 1:100) and mouse anti-ubiquitin (Cell Signaling Technology, 3936S; 1:500). Cells were then stained with secondary antibody in PBS for 1 h and washed with PBS three times. Secondary antibodies were purchased from Invitrogen (Alexa Fluor 488 goat anti-rabbit IgG, A11008; Alexa Fluor 546 goat anti-rabbit IgG, A11035; Alexa Fluor 488 goat anti-mouse IgG, A10680; Alexa Fluor 546 goat anti-mouse IgG, A11003; 1:500). Confocal fluorescence microscopy was performed on a Nikon C2+ Confocal Microscope System using standard filter sets, laser lines, Plan Apo 100×/1.4 oil OFN25 DIC N2 and CFI 10×/22 lenses. Imaging medium was Immersion Oil Type N (Nikon). Image acquisition and processing were performed using NIS-Elements software (Laboratory Imaging).

Sedimentation assay
Purified proteins were pre-cleared via high-speed centrifugation and mixed in the indicated combinations. The final volume of each mixture was 50 μL. After 5 min settling down at room temperature, each mixture was subjected to sedimentation at 12,652× g for 15 min. Then, the supernatant and pellet were immediately separated into different tubes, and each fraction was supplemented with sedimentation buffer (150 mM NaCl, 40 mM Tris-HCl, pH 7.4, 10% glycerol, 1 mM DTT) to give a final volume of 50 μL. Finally, the sedimentation samples were analyzed by western blotting.

FRAP
FRAP experiments were performed on a NIKON A1 microscope with a 60× oil immersion objective. p62 bodies in vivo were bleached for 3 s using a laser intensity of 70% at 480 nm (for GFP) or 561 nm (for tdTomato). Recovery was recorded for the indicated time. The fluorescence intensity of the photobleached area was normalized to the intensity of the unbleached area.

Live-cell imaging
Transfected cells were re-plated in Lab Tek Chambered cover glasses (NUNC) for 12–18 h before imaging, and cells were maintained at 37 °C under 5% CO_2. Images were acquired using Andor high speed confocal Dragonfly microscopy (Belfast, UK) with a 60× oil immersion lens. All live-cell imaging experiments were repeated at least 3 times.
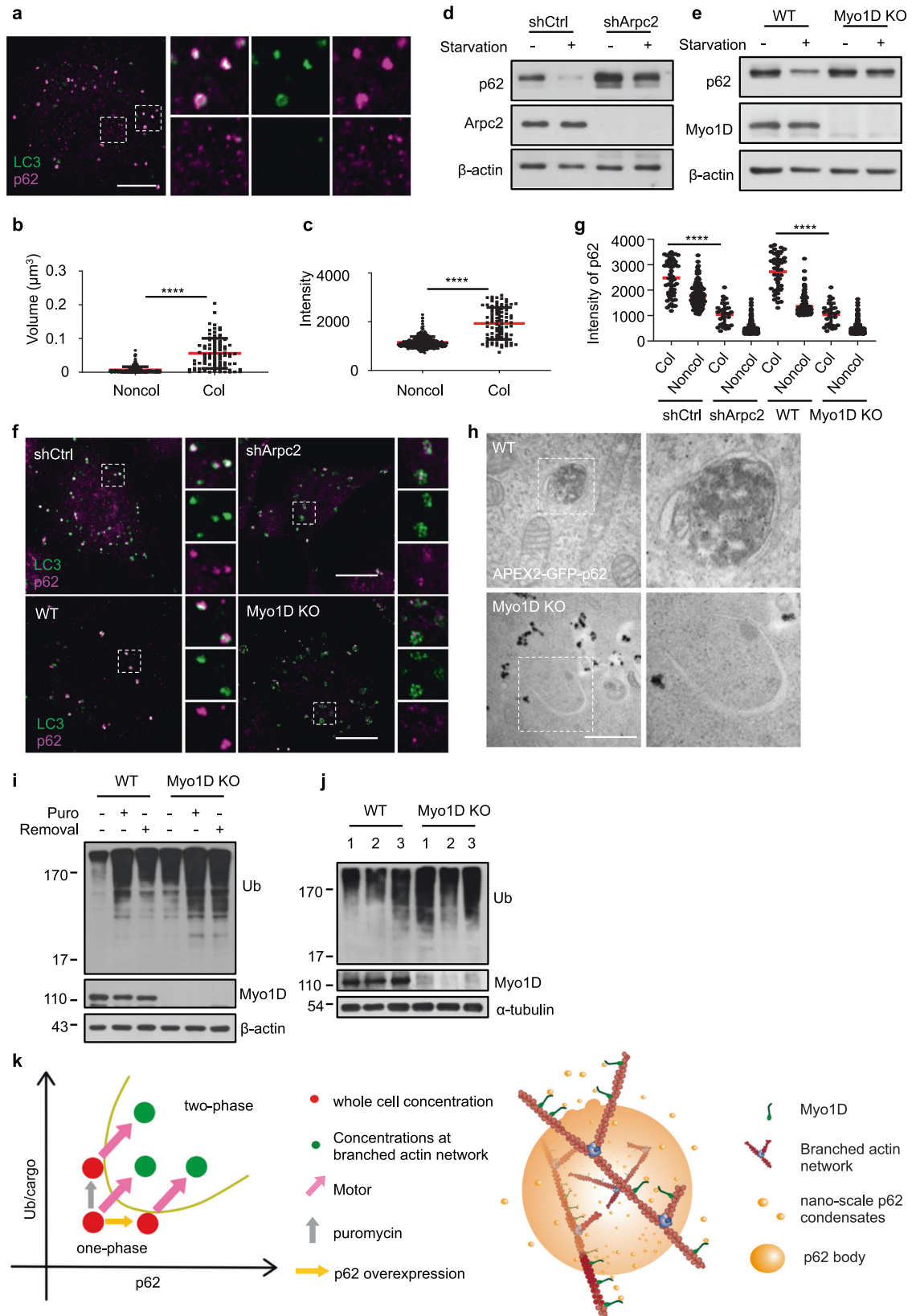
Electron microscopy

Cells cultured in 3.5 cm dishes were fixed by 1:1 (v/v) 2.5% glutaraldehyde and DMEM for 5 min at room temperature. The liquid was removed and the cells were incubated in 2.5% glutaraldehyde for 45 min at 4 ℃. The cells were then washed twice with 0.1 M sodium cacodylate buffer (pH 7.3) for 5 min at 4 ℃, and treated with 20 mM glycine for 5 min at 4 ℃. After three washes for 5 min at 4 ℃, the cells were incubated with 1 mg/mL DAB for 2 min at room temperature, then H_2O_2 was added (0.03% (v/v)) and the

Fig. 5 **The branched actin network regulates autophagy by harnessing p62 phase condensation. a** NRK cells were starved for 4 h, and then stained with antibodies against LC3 and p62. The left panel shows the colocalization of p62 and LC3. Right panels show enlarged p62 structures that were either LC3-positive (upper panels) or LC3-negative (lower panels). Scale bar, 10 μm. **b**, **c** Size (**b**) or intensity (**c**) variation of p62 bodies that are colocalized (Col) or non-colocalized (Noncol) with LC3 in **a**. Size was quantified as volume (μm³). *P*-values were calculated using the two-tailed unpaired *t*-test (*n* = 3). ****P* < 0.0001. **d** Cells transfected with non-targeting control shRNA (shCtrl) or Arpc2 KD shRNA (shArpc2) were starved with DPBS (STA) for 2 h, and then the cell lysates were analyzed by western blotting with antibodies against p62 and β-actin. **e** WT cells or Myo1D KO cells were starved with DPBS (STA) for 2 h, and then the cell lysates were analyzed by western blotting with antibodies against p62 and β-actin. **f** Cells transfected with shCtrl or shArpc2 or Myo1D KO cells were starved for 4 h, and then stained with antibodies against p62 and LC3 followed by confocal microscopy analysis. Right panels show enlarged p62 structures which were LC3 positive. Scale bar, 10 μm. **g** Intensity variation of p62 bodies that are colocalized or non-colocalized with LC3 in each group in **f** after nutrient starvation. *P*-values were calculated using the two-tailed unpaired *t*-test (*n* = 3). **P* < 0.05; ****P* < 0.0001. **h** TEM images showing the DAB staining pattern in WT NRK cells and Myo1D KO cells transiently expressing APEX2-GFP-p62 followed by starvation for 4 h. Scale bar, 1 μm. **i** WT and Myo1D KO NRK cells were treated with 1 mg/mL puromycin for 8 h. After puromycin washout, the cells were cultured in normal conditions for 16 h, and then the cell lysates were analyzed by western blotting with antibodies against ubiquitin and Myo1D. **j** Brain lysates of WT and Myo1D KO mice were analyzed by western blotting with antibodies against ubiquitin and Myo1D. **k** Left, phase diagram as a function of the branched actin networks and motor proteins for condensate formation. Right, a working model showing that the branched actin network and Myo1D-mediated active transportation drive the condensation of p62 bodies.

incubation continued for 15 min. After three more washes, the cells were observed by electron microscopy (Zeiss EM 10 transmission electron microscope). All the solutions above were in 0.1 M sodium cacodylate buffer (pH 7.3).

Protein expression and purification

pCAG-strep-Myosin1D vector was transfected into HEK293F cells using a polyethylenimine-based transfection protocol.[40] 2 mg DNA was used for transfection of 1 L HEK293F cells. Cells were collected 3 days after transfection and lysed using a Dounce tissue grinder (100 strokes) in buffer containing 25 mM Tris-HCl (pH 8.0), 150 mM NaCl and protease inhibitor cocktail (Roche, 4693132001). After centrifugation at 30,000× *g* for 1 h at 4 °C, the pellet was lysed in buffer containing 25 mM Tris-HCl (pH 8.0), 150 mM NaCl, 2% Fos-Choline-12 (Anatrace, F308) and protease inhibitor cocktail for 2 h at 4 °C. After centrifugation at 30,000× *g* for 30 min, the supernatant was loaded onto a column containing Strep-Tactin resin (IBA, 2-1202) and incubated for 1 h at 4 °C. The resin was then washed four times. The protein was eluted with 10 mM desthiobiotin (Sigma Aldrich, D1411) and further purified by gel filtration on Superdex 200. Expression and purification of mCherry-p62-WT, ΔPB1 mCherry-p62, and Ub8 have been described.[21] Myo1D IQ-TH1, Myo1D IQ, Myo1D Motor, Myo1D Motor-IQ or Myo1D TH1 were expressed in *Escherichia coli* BL21 cells in LB medium at 16 °C for 20 h. Protein expression was induced by 0.25 mM IPTG (final concentration) at OD600 of ~0.6. Recombinant proteins were purified using a nickel-nitrilotriacetic acid (NTA) agarose affinity column followed by size-exclusion chromatography (Superdex 200) with a buffer containing 50 mM Tris-HCl (pH 7.4), 150 mM NaCl, 1 mM EDTA, and 1 mM DTT. For FL Myo1D, proteins were expressed by using the Bac-to-Bac expression system. In brief, Sf9 cells were grown in sf-900 II SFM medium to a density of 2 × 10⁶ cells/mL and incubated with virus harboring FL Myo1D construct. After 60 h, cells were collected, lysed by freeze-thaw cycles, and centrifuged at 4 °C. The soluble fraction was bound in batches to nickel-NTA agarose, and the resin was washed. His6-tagged Myo1D was eluted with 20 mM Tris, 0.1 M NaCl, and 250 mM imidazole (pH 8.0).

In vitro phase separation assay

The droplet formation assay was performed using purified proteins fused with mCherry tag or labeled with Alexa Fluor 405 or 568 in TIRF buffer (1 mM MgCl₂, 50 mM KCl, 1 mM EGTA, 10 mM imidazole, pH 8.0, 0.2 mM ATP, 100 mM DTT, 100 μg/mL glucose oxidase, 20 μg/mL catalase, 0.2% BSA, and 0.5% methylcellulose). For protein labeling, the indicated dyes were incubated with Ub8 and Myo1D at a 1:1 molar ratio at room temperature for 1 h. Labeled proteins were concentrated and loaded onto an SD200 column to remove free dye and finally stored at –80 °C. For the assays, 5% labeled protein was mixed with unlabeled protein.

In vitro reconstitution of p62 bodies

To initiate actin polymerization, we added 1 μM actin (50% Oregon-green labeled), 100 nM Arp2/3 complex, 600 nM capping protein (CapZ), and 300 nM PWCA to Lab Tek chambered cover glasses (NUNC). In the focal plane of the chamber, we observed robust actin polymerization by TIRF microscopy. Then, 0.5 μM mCherry-p62, 3 μM Ub8 and 10 μM Myo1D were added to the solution and TIRF imaging was continued.

Generation and analysis of Myo1D KO mice

We use CRISPR/Cas9 technology to modify the *Myo1d* gene. The brief process is as follows: sgRNA (gRNA1: TGCAGTGTTGCTCTAGTCCA; gRNA2: ATAGGATGCTCTGGTGTCGC) was transcribed in vitro. Cas9 and sgRNA were microinjected into the fertilized eggs of C57BL/6J mice. Fertilized eggs were transplanted to obtain positive F0 mice which were confirmed by PCR and sequencing. A stable F1 generation mouse model was obtained by mating positive F0 generation mice with C57BL/6J mice. Mice were purchased from GemPharmatech Co., Ltd. For each group, at least eight mice were sacrificed for subsequent analyses. For all experiments, male and female mice were used. All mice for each line were littermates and housed on a 12 h light/dark cycle with ad libitum food and water. All mouse experiments were approved by the Animal Ethics Committee of Xinjiang Medical University and carried out in accordance with institutional guidelines. Brain tissues from 12-week-old *Myo1d*⁻/⁻ mice were lysed on ice in lysis buffer and protease inhibitor mixture (Roche, 4693132001). Protein concentrations were determined using a protein assay kit (Thermo Fisher Scientific, 23227). Equal amounts of protein from each sample were used for western blotting.

Statistical analysis

Statistical analysis was performed using GraphPad Prism 8. For Supplementary information, Fig. S7c, p62 bodies were identified automatically as surfaces in Imaris 9.6 (Oxford Instruments). Five cells from each group were selected for analysis. The same thresholds were applied to each cell. The areas of surfaces in each group were quantified and compared. The results were plotted and *P*-values were calculated in GraphPad using the two-tailed unpaired *t*-test. For Fig. 5b, c, g, LC3 signals were identified automatically as surfaces with shortest distance in Imaris. p62 signals were identified as surfaces and classified by the shortest distance to the surfaces of LC3 (Col: ≤ 0.1 μm, Noncol: ≥ 0.1 μm). The threshold between groups was adjusted to ensure that there was overlap between the surfaces of LC3 and p62 puncta. In each group, the intensity and volume of p62 surfaces that were colocalized and non-colocalized with LC3 were quantified and compared. The results were plotted and *P*-values were calculated in GraphPad using the two-tailed unpaired *t*-test. For Fig. 4i, actin signals were identified automatically as surfaces with shortest distance in Imaris. p62 signals were identified as surfaces and classified inside/outside by the shortest distance to the surfaces of actin, and the threshold of classification is adjusted manually for the best representation. The area of p62 surfaces were quantified and compared between different groups. We compare the area of: (1) p62 puncta in and out of actin branch, (2) p62 puncta in actin branch with and without Myo1D, (3) p62 puncta in actin branch and on actin filaments with Myo1D. The results were plotted and *P*-values were calculated in GraphPad using the two-tailed unpaired *t*-test.

REFERENCES

1. Banani, S. F., Lee, H. O., Hyman, A. A. & Rosen, M. K. Biomolecular condensates: Organizers of cellular biochemistry. *Nat. Rev. Mol. Cell Biol.* **18**, 285–298 (2017).
2. Brangwynne, C. P. et al. Germline P granules are liquid droplets that localize by controlled dissolution/condensation. *Science* **324**, 1729–1732 (2009).
3. Banani, S. F. et al. Compositional control of phase-separated cellular bodies. *Cell* **166**, 651–663 (2016).

4. Li, P. et al. Phase transitions in the assembly of multivalent signalling proteins. *Nature* **483**, 336–340 (2012).

5. Wu, X., Cai, Q., Feng, Z. & Zhang, M. Liquid-liquid phase separation in neuronal development and synaptic signaling. *Dev. Cell* **55**, 18–29 (2020).

6. Wu, X. et al. RIM and RIM-BP form presynaptic active-zone-like condensates via phase separation. *Mol. Cell* **73**, 971–984.e975 (2019).

7. Zeng, M. et al. Phase separation-mediated TARP/MAGUK complex condensation and AMPA receptor synaptic transmission. *Neuron* **104**, 529–543.e526 (2019).

8. Liu, Z. et al. Par complex cluster formation mediated by phase separation. *Nat. Commun.* **11**, 2266 (2020).

9. Case, L. B., Zhang, X., Ditlev, J. A. & Rosen, M. K. Stoichiometry controls activity of phase-separated clusters of actin signaling proteins. *Science* **363**, 1093–1097 (2019).

10. Shimobayashi, S. F., Ronceray, P., Sanders, D. W., Haataja, M. P. & Brangwynne, C. P. Nucleation landscape of biomolecular condensates. *Nature* **599**, 503–506 (2021).

11. Minton, A. P. Holobiochemistry: The effect of local environment upon the equilibria and rates of biochemical reactions. *Int. J. Biochem.* **22**, 1063–1067 (1990).

12. Jalihal, A. P. et al. Hyperosmotic phase separation: Condensates beyond inclusions, granules and organelles. *J. Biol. Chem.* **296**, 100044 (2021).

13. Woodruff, J. B. et al. The centrosome is a selective condensate that nucleates microtubules by concentrating tubulin. *Cell* **169**, 1066–1077.e1010 (2017).

14. Su, X. et al. Phase separation of signaling molecules promotes T cell receptor signal transduction. *Science* **352**, 595–599 (2016).

15. Jiang, H. et al. Phase transition of spindle-associated protein regulate spindle apparatus assembly. *Cell* **163**, 108–122 (2015).

16. Hernandez-Vega, A. et al. Local nucleation of microtubule bundles through tubulin concentration into a condensed tau phase. *Cell Rep.* **20**, 2304–2312 (2017).

17. Wiegand, T. & Hyman, A. A. Drops and fibers — how biomolecular condensates and cytoskeletal filaments influence each other. *Emerg. Top. Life Sci.* **4**, 247–261 (2020).

18. Ditlev, J. A. et al. A composition-dependent molecular clutch between T cell signaling condensates and actin. *Elife* **8**, e42695 (2019).

19. Mi, N. et al. CapZ regulates autophagosomal membrane shaping by promoting actin assembly inside the isolation membrane. *Nat. Cell Biol.* **17**, 1112–1123 (2015).

20. Kast, D. J., Zajac, A. L., Holzbaur, E. L., Ostap, E. M. & Dominguez, R. WHAMM directs the Arp2/3 complex to the ER for autophagosome biogenesis through an actin comet tail mechanism. *Curr. Biol.* **25**, 1791–1797 (2015).

21. Saydmohammed, M. et al. Vertebrate myosin 1d regulates left-right organizer morphogenesis and laterality. *Nat. Commun.* **9**, 3381 (2018).

22. Fujioka, Y. et al. Phase separation organizes the site of autophagosome formation. *Nature* **578**, 301–305 (2020).

23. Agudo-Canalejo, J. et al. Wetting regulates autophagy of phase-separated compartments and the cytosol. *Nature* **591**, 142–146 (2021).

24. Turco, E. et al. FIP200 claw domain binding to p62 promotes autophagosome formation at ubiquitin condensates. *Mol. Cell* **74**, 330–346.e11 (2019).

25. Lystad, A. H. & Simonsen, A. Assays to monitor aggrephagy. *Methods* **75**, 112–119 (2015).

26. Nolen, B. J. et al. Characterization of two classes of small molecule inhibitors of Arp2/3 complex. *Nature* **460**, 1031–1034 (2009).

27. Riedl, J. et al. Lifeact: a versatile marker to visualize F-actin. *Nat. Methods* **5**, 605–607 (2008).

28. Hung, V. et al. Spatially resolved proteomic mapping in living cells with the engineered peroxidase APEX2. *Nat. Protoc.* **11**, 456–475 (2016).

29. Blanchoin, L., Boujemaa-Paterski, R., Sykes, C. & Plastino, J. Actin dynamics, architecture, and mechanics in cell motility. *Physiol. Rev.* **94**, 235–263 (2014).

30. Michelot, A. & Drubin, D. G. Building distinct actin filament networks in a common cytoplasm. *Curr. Biol.* **21**, R560–R569 (2011).

31. McIntosh, B. B. & Ostap, E. M. Myosin-I molecular motors at a glance. *J. Cell Sci.* **129**, 2689–2695 (2016).

32. Benesh, A. E. et al. Differential localization and dynamics of class I myosins in the enterocyte microvillus. *Mol. Biol. Cell* **21**, 970–978 (2010).

33. Brandstaetter, H., Kendrick-Jones, J. & Buss, F. Myo1c regulates lipid raft recycling to control cell spreading, migration and Salmonella invasion. *J. Cell Sci.* **125**, 1991–2003 (2012).

34. Campellone, K. G., Webb, N. J., Znameroski, E. A. & Welch, M. D. WHAMM is an Arp2/3 complex activator that binds microtubules and functions in ER to Golgi transport. *Cell* **134**, 148–161 (2008).

35. Zhao, Y. G. & Zhang, H. Phase separation in membrane biology: The interplay between membrane-bound organelles and membraneless condensates. *Dev. Cell* **55**, 30–44 (2020).

36. Shin, Y. & Brangwynne, C. P. Liquid phase condensation in cell physiology and disease. *Science* **357**, eaaf4382 (2017).

37. Chen, X. D., Wu, X. D., Wu, H. W. & Zhang, M. J. Phase separation at the synapse. *Nat. Neurosci.* **23**, 301–310 (2020).

38. Huang, W. Y. C. et al. A molecular assembly phase transition and kinetic proofreading modulate Ras activation by SOS. *Science* **363**, 1098–1103 (2019).

39. Maharana, S. et al. RNA buffers the phase separation behavior of prion-like RNA binding proteins. *Science* **360**, 918–921 (2018).

40. Huang, Y. et al. Migrasome formation is mediated by assembly of micron-scale tetraspanin macrodomains. *Nat. Cell Biol.* **21**, 991–1002 (2019).

ACKNOWLEDGEMENTS

AUTHOR CONTRIBUTIONS

N.M. conceived the study; N.M. and P.L. wrote the manuscript and supervised the project; X. Feng, W.D., M.D. and X.X. performed most of the experiments. M.M., X.L., D. S., Q.X., Y.A. and Q.C. contributed to parts of the experiments. Y.L. helped with the electron microscopy. L.Y. provided insightful suggestions. W.Z. and W.W. helped with Imaris analysis. Y.Z., J.S., S.H. and X. Fu helped with actin polymerization. All the authors discussed and commented on the manuscript.

COMPETING INTERESTS

ADDITIONAL INFORMATION